Localized surface plasmon resonance interaction with Er^{3+}-doped tellurite glass

V. A. G. Rivera,[1,*] S. P. A. Osorio,[1] Y. Ledemi,[2] D. Manzani,[2] Y. Messaddeq,[2] L. A. O. Nunes,[1] and E. Marega Jr.[1]

[1]*Instituto de Física de São Carlos - INOF, USP, Caixa Postal 369, 13560-970, São Carlos – SP, Brasil*
[2]*Instituto de Química de Araraquara – UNESP, Araraquara – SP, Brasil*
**garcia@ursa.ifsc.usp.br*

Abstract: We show the annealing effect on silver and Erbium- doped tellurite glasses in the formation of nanoparticles (NPs) of silver, produced by the reduction of silver ($Ag^{+}\rightarrow Ag^{0}$), aiming to an fluorescence enhancement. The absorption spectra show typical Localized Surface Plasmon Resonance (LSPR) band of Ag^{0} NP in addition to the distinctive absorption peaks of Er^{3+} ions. Both observations demonstrate that the photoluminescence enhancement is due to the coupling of dipoles formed by NPs with the Er^{3+} $^{4}I_{13/2}\rightarrow{}^{4}I_{15/2}$ transition. This plasmon energy transfer to the Er^{3+} ions was observed in the fluorescence spectrum with a blue-shift of the peaks.

OCIS code: (240.6680) Surface plasmons; (300.6280) Spectroscopy, fluorescence and luminescence; (060.4510) Optical communications.

References and links

1. P. N. Prasad, *Nanophotonics* (Wiley, New York, 2004).
2. C. Li, Z. Quan, J. Yang, P. Yang, and J. Lin, "Highly uniform and monodispersive β-$NaYF_4$:Ln^{3+} (Ln = Eu, Tb, Yb/Er and Yb/Tm) hexagonal microprism crystals: Hydrothermal synthesis and luminescent properties," Inorg. Chem. **46**(16), 6329–6337 (2007).
3. K. R. Brown, D. G. Walter, and M. J. Natan, "Seeding of colloidal Au nanoparticle solutions. 2. Improved control of particle size and shape," Chem. Mater. **12**(2), 306–313 (2000).
4. T. Som, and B. Karmakar, "Nanosilver enhanced upconversion fluorescence of erbium ions in Er^{3+}: Ag-antimony glass nanocomposites," J. Appl. Phys. **105**(1), 013102 (2009).
5. S. Kim, J. Jin, Y. J. Kim, I. Y. Park, Y. Kim, and S. W. Kim, "High-harmonic generation by resonant plasmon field enhancement," Nature **453**(7196), 757–760 (2008).
6. S. Kühn, U. Håkanson, L. Rogobete, and V. Sandoghdar, "Enhancement of single-molecule fluorescence using a gold nanoparticle as an optical nanoantenna," Phys. Rev. Lett. **97**(1), 017402 (2006).
7. O. L. Malta, P. O. Santa-Cruz, G. F. de Sá, and F. Auzel, "Fluorescence enhancement induced by the presence of small silver particles in Eu^{3+} doped materials," J. Lumin. **33**(3), 261–272 (1985).
8. V. A. G. Rivera, E. Rodriguez, E. F. Chillcce, C. L. Cesar, and L. C. Barbosa, "Waveguide produced by fiber on glass method using Er3+-doped tellurite glass," J. Non-Cryst. Solids **353**(4), 339–343 (2007).
9. V. A. G. Rivera, E. F. Chillcce, E. Rodriguez, C. L. Cesar, and L. C. Barbosa, "Planar waveguides by ion exchange in Er3+-doped tellurite glass," J. Non-Cryst. Solids **352**(5), 363–367 (2006).
10. S. Tanabe, T. Ohyagi, N. Soga, and T. Hanada, "Compositional dependence of Judd-Ofelt parameters of Er^{3+} ions in alkali-metal borate glasses," Phys. Rev. B Condens. Matter **46**(6), 3305–3310 (1992).
11. T. Catunda, L. A. O. Nunes, A. Florez, Y. Messaddeq, and M. A. Aegerter, "Spectroscopic properties and upconversion mechanisms in Er^{3+}-doped fluoroindate glasses," Phys. Rev. B Condens. Matter **53**(10), 6065–6070 (1996).
12. Y. D. Huang, M. Mortier, and F. Auzel, "Stark levels analysis for Er^{3+}-doped oxide glasses: germanate and silicate," Opt. Mater. **15**(4), 243–260 (2001).
13. B. R. Judd, "Optical absorption intensities of rare-earth ions," Phys. Rev. **127**(3), 750–761 (1962).
14. F. Vallé, *In Nanoscience: Nanomaterials and Nanochemistry*, C. Dupas and M. Lahmani, Eds.; (Springer, Berlin, 2008), 197 pages.
15. D. D. Evanoff, R. L. White, and G. Chumanov, "Measuring the Distance Dependence of the Local Electromagnetic Field from Silver Nanoparticles," J. Phys. Chem. B **108**(5), 1522–1524 (2004).
16. H. Baida, P. Billaud, S. Marhaba, D. Christofilos, E. Cottancin, A. Crut, J. Lermé, P. Maioli, M. Pellarin, M. Broyer, N. Del Fatti, F. Vallée, A. Sánchez-Iglesias, I. Pastoriza-Santos, and L. M. Liz-Marzán, "Quantitative

#134395 - $15.00 USD Received 31 Aug 2010; revised 11 Oct 2010; accepted 14 Oct 2010; published 19 Nov 2010

determination of the size dependence of surface plasmon resonance damping in single Ag@SiO(2) nanoparticles," Nano Lett. **9**(10), 3463–3469 (2009).
17. C. Voisin, N. Del Fatti, D. Christofilos, and F. J. Valleé, "Ultrafast electron dynamics and optical nonlinearities in metal nanoparticles," Phys. Chem. B **105**(12), 2264–2280 (2001).
18. F. Hache, D. Ricard, and C. J. Flytzanis, "Optical nonlinearities of small metal particles: surface-mediated resonance and quantum size effects," J. Opt. Soc. Am. B **3**(12), 1647–1655 (1986).
19. F. Le, D. W. Brandl, Y. A. Urzhumov, H. Wang, J. Kundu, N. J. Halas, J. Aizpurua, and P. Nordlander, "Metallic nanoparticle arrays: a common substrate for both surface-enhanced Raman scattering and surface-enhanced infrared absorption," ACS Nano **2**(4), 707–718 (2008).
20. JCPDS Card File No. 4–0783.
21. G. S. Ofelt, "Intensities of Crystal Spectra of Rare-Earth Ions," J. Chem. Phys. **37**(3), 511–520 (1962).
22. H. Mertens, and A. Polman, "Plasmon-enhanced erbium luminescence," Appl. Phys. Lett. **89**(21), 211107 (2006).

1. Introduction

The interaction of light with rare-earth (RE) doped glasses containing metallic NPs have been attracting large attention due to their relevance for a variety of applications such as colored displays and amplifier waveguides for telecommunications [1]. The Erbium-doped tellurite glass is a well known host matrix that plays an important role as optical amplifiers and optic fibers due to a variety of potential applications, and high solubility for RE ions [2]. Moreover, they have attracted much interest in optoelectronic and photonic applications because the emission in the telecommunication optical window is due to the 4f↔4f transitions, not only the $^4I_{13/2}\rightarrow{}^4I_{15/2}$ transition, but also the upconversion transition. These transitions intensities depend strongly on the nature and structure of chemical environment around Er^{3+} ion. On the other hand, NPs can be a candidate for enhancement fluorescence studies, as showing by several efforts devoted on the study and exploitation of Localized Surface Plasmons Resonance (LSPR) and local field properties of metal NPs and their potential applications. However, the controlled production of anisotropic NPs embedded in glasses matrix is a current challenging with promissory applications [3].

2. Samples preparation and the experimental setup

The glasses samples of 10 g weight were obtained using the following starting composition: $75TeO_2$–$2GeO_2$–$15Na_2O$–$7ZnO$–$1Er_2O_3$-xAgCl (mol%). The 1 mol% Er_2O_3 concentration is equivalent to 10000 ppm in weight of erbium, where x = 0.25 and 0.50 for the samples TE025-Y and TE050-Y respectively, and Y is the annealing time at a fixed temperature at 300 °C (Y = 2.5, 5.0, 7.5 and 10.0 hours).

The glass samples were prepared by the conventional technique of melt-quenching. A gold crucible containing the glass constituents was placed in a furnace from ambient temperature up to 750 °C, where it remained for 2 h. After melting, the glass is quenched and cooled to ambient temperature. Finally, to reduce internal stresses caused by the thermal shock, the glass samples underwent annealing as mentioned previously. Silver NPs embedded in this host matrix were synthesized according to the annealing time. The final samples were cut in square pieces of $10\times 30\times 1.5$ mm^3 approximately and polished until obtaining an adequate transparency for optical characterization.

The different annealing times Y results in the formation of different NPs sizes with different distances between them dispersed in the vitreous matrix. TEM photograph was done using a Philips-CM120 operating at 200 kV. Through XRD measurements, the average NP size was calculated using Scherre's formula: $d = 0.9\lambda / \left\{ FWHM\cos\left(2\theta_{peak}\right)\right\}$, where l is the wavelength of XRD (Cu *K*a = 1.5418 Å), FWHM is the full width at half maximum 2θ. The XRD was performed by a Rigaku-Rota Flex mod. RU200B, with 2θ varying from 10° to 80° with step of 0.02°, using Ni filter, at 40 mA and 40 kV. In our calculations it is assumed that the NPs are perfectly spherical. We also have calculated the concentration N (atoms/cm^3) of Ag and the distance between various species (mean inter-ionic distance r_m) in each NP by the

#134395 - $15.00 USD Received 31 Aug 2010; revised 11 Oct 2010; accepted 14 Oct 2010; published 19 Nov 2010

relation: $N\left(\text{ions or atoms/cm}^3\right) = A \times N_0 \times \rho / M_{av}$, and $r_m = \left(1/N\right)^{1/3}$ [4], where A is the ion or atom per cent, N_0 is Avogadro's number, ρ is glass density (g/cm^3), and M_{av} glass average molecular weight. The density of the glass samples was measured by the Archimedes method using distilled water as immersion medium, obtained in average $\rho_{\text{TE025-Y}} = 5.1 \pm 0.1$ and $\rho_{\text{TE050-Y}} = 5.3 \pm 0.1$. The characteristic temperatures of the glass, the glass transition temperature T_g, the temperature of the onset of crystallization T_x, and the maximum crystallization temperature T_c were determined by Differential Scanning Calorimetry (DSC) with heating rates of 10 °C/min. The results are show in the Table 1.

Absorption spectroscopy was performed by a Perkin–Elmer Lambda 900 UV/Vis/NIR spectrophotometer, in the range from 400 to 1800 nm at room temperature. Luminescence spectra were performed using a 980 nm diode laser of 2.0 W of power, an InGaAs detector and lock-in technique. For measuring the $^4I_{13/2}$ lifetime, the samples were irradiated with a 980-nm-laser diode with a pulse train of 50 μs up and with dead time of 100 ms. The emission signal was measured by a 400 MHz oscilloscope (Tektronix TDS 380).

Based on the thermal parameters obtained for the glass (see Table 1), the proposed annealing temperature was 300 °C (just up T_g) to perform the NPs formation.

Table 1. Some calculated physical properties and relative intensities of the luminescence enhancement of the samples. Besides as well glass transition temperatures T_g

Sample	T_g (°C) ± 0.3	N_{Ag0} (atoms/cm^3) ± 0.03 × 10^x	η ± 0.04	r_m/d ± 0.01
TE025-2.5	284.2	5.21×10^{19}	8.77	0.13
TE025-5.0	283.7	5.21×10^{19}	8.57	0.13
TE025-7.5	283.4	5.19×10^{19}	9.52	0.12
TE025-10.0	283.2	5.27×10^{19}	10.60	0.10
TE050-2.5	282.5	1.06×10^{20}	9.18	0.12
TE050-5.0	281.8	1.08×10^{20}	10.03	0.11
TE050-7.5	282.1	1.09×10^{20}	7.37	0.16
TE050-10.0	283.1	1.08×10^{20}	8.86	0.13

x = same order of power.

3. Results and discussions

Tellurite glass doped Er^{3+} ions and co-doped with NPs can induce significant enhancement of the Erbium fluorescence due to long-range electromagnetic interaction between the plasmons of the Ag NPs in the host medium. This strong enhancement of electromagnetic fields is essential in nonlinear optics effects, and allowed achieve to high values of electromagnetic field enhancement through the excitation of LSP [5,6]. A LSP is a free electrons oscillation of a metallic particle, whose frequency of resonance is the plasma frequency (w_P) tuned by the size and shape of the particle. Such oscillations are caused by the interaction between the incident radiation and the NPs, these oscillations are dependent on the shape and size of NPs.

Thus, the enhancement obtained with these NPs is due to the formation of electric dipoles (ED) which generates a polarization given by $\vec{P}_{NP} = qeN'\vec{x}$, where $\vec{x}$ is the distance between each NP, $q = \pi d^3/6$ is the NP specific volume, N' is the conduction electrons density, and e is the electronic charge. Therefore, a modification in the local electric field is produced by these dipoles that can be understood as a local field correction. Now, the interaction of a homogeneous NP of diameter d (d<<l) with electromagnetic field will be considered in two regimes: First, for large particles (d > 20 nm), where the quasi-static approximation breaks down due to absorption effects, and second, the regime of very small NP $d \leq 20$ nm, where the particle dimensions are appreciably smaller than the mean free path of its oscillating electrons.

Using the results obtained by O.L. Malta et al [7], the effective electric field can be written as: $\vec{E}_{eff} = \left(\varepsilon_0 + 2\right)\left(1 + q\omega_P^2 / \left\{3\varepsilon_0\left[\left(1-q\right)\left(\omega_P^2/3\varepsilon_0\right) - \omega^2 + i\gamma\omega\right]\right\}\right)\vec{E}_0/3$, where g is the

#134395 - $15.00 USD Received 31 Aug 2010; revised 11 Oct 2010; accepted 14 Oct 2010; published 19 Nov 2010

damping the resonance, ε_0 is the dielectric constant in the presence of an external electromagnetic field of amplitude E_0. In the presence of an electromagnetic field we have LSPR which forms EDs separated by different distance $\bar{r}$, some of which will contribute to the luminescence enhancement.

For the 1.55 μm Er^{3+} emission, used for optical amplification in telecommunications [8,9], the analysis of transitions between the $^4I_{13/2}$ and $^4I_{15/2}$ manifolds [10,11] induced most of the studies and only few papers have been dealt with the transitions between Stark levels [12]. The measurement of Er^{3+} absorption and emission spectra in these glasses, shown in the Fig. 1 and Fig. 2, allowed determine the position and width of Stark levels for Er^{3+} ions. We observe that in the Fig. 1 (a) it is not possible to observe the band related to the LSPR due to the little quantity of Ag co-doped. Therefore, two samples were prepared with the same quantities of Ag co-doped used in the other glasses with different annealing time, but without Er^{3+} ions in order to be able to detect and to observe plasmon wavelength λ_p, just as it is shown in the Fig. 1(b) and is compared with absorption spectrum of glass without Ag co-doped.

Assuming that the Er^{3+} ions may occupy different sites in the host, a direct coupling between the excited states of the Er^{3+} ions and the Ag NPs modifies the Stark levels energies, see Fig. 3. In this frame, the quantitative determination of the properties is obtained through proper group symmetry operations. As the NPs just give a contribution to the local field when the light is present, the oscillator strength ($P_{strength}$) of a spectral line, corresponding to transition from the ion ground level *i* to the component *f* of the excited level, is given by:

$$P_{strength} = \chi\left[\frac{8\pi^2 m\upsilon}{3h(2J+1)}\right]\left(\sum\left|\langle i|D^{(1)}_{q\ nearest-neighbor}|f\rangle\right|^2 + \sum\left|\langle i|D^{(1)}_{q',\,Ag-NP}|f\rangle\right|^2\right) \quad (1)$$

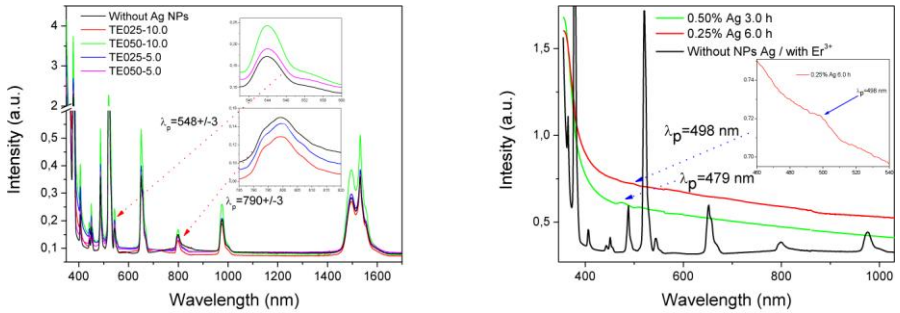

(a) (b)

Fig. 1. (a) Absorption spectra of some samples. The two figures inserted show the observation of LSPR to different glasses. In this sense, the absorption band related to LSPR is not observed because the amount of the NPs is not enough to originate a strong peak. (b) In this picture observed the Ag λ_p from the absorption spectra of glasses without Er^{3+} ions in to different annealing time, besides the glass doped with Er^{3+} ions without Ag NPs. Into figure the inset is show a zoom the spectrum from the glass with 0.25% Ag doped.

This equation is modified, for the second term into parenthesis, from the theory of Judd [13], and represents the ED transition due to SPR of Ag NP, where m is the mass of an electron, h is the Planck constant, υ is the frequency of the line. The factor χ is an adjustable factor that depends on the refractive index of the medium in which the Er^{3+} ions are embedded, and J is the total angular momentum. To obtain non vanishing matrix elements of the components $D^{(1)}_{q',\,Ag-NP}$ it is necessary to admix into $\langle i|$ and $|f\rangle$ other states of opposite parity. This occur for q' = 2, 4 and 6. Thus, the initial and final states is:

$$\langle i| = \langle\varphi_i| + \sum_\beta \langle\varphi_i|V_{crys}|\varphi_\beta\rangle / (E_i - E_\beta)\langle\varphi_\beta|,$$

#134395 - $15.00 USD Received 31 Aug 2010; revised 11 Oct 2010; accepted 14 Oct 2010; published 19 Nov 2010

and

$$|f\rangle = |\varphi_f\rangle + \sum_{\beta} \langle \varphi_\beta | V_{crys} | \varphi_f \rangle / (E_f - E_\beta) | \varphi_\beta \rangle,$$

then:

$$\langle i | \vec{P} + \vec{P}_{NP} | f \rangle = \sum_{\beta} \{ \langle \varphi_i | V_{crys} | \varphi_\beta \rangle \langle \varphi_\beta | \vec{P} | \varphi_f \rangle / (E_i - E_\beta)$$

$$+ \langle \varphi_i | \vec{P} | \varphi_\beta \rangle \langle \varphi_\beta | V_{crys} | \varphi_f \rangle / (E_f - E_\beta) + \langle \varphi_i | V_{crys} | \varphi_\beta \rangle \langle \varphi_\beta | \vec{P}_{NP} | \varphi_f \rangle / (E_i - E_\beta) + \langle \varphi_i | \vec{P}_{NP} | \varphi_\beta \rangle \langle \varphi_\beta | V_{crys} | \varphi_f \rangle / (E_f - E_\beta) \}.$$

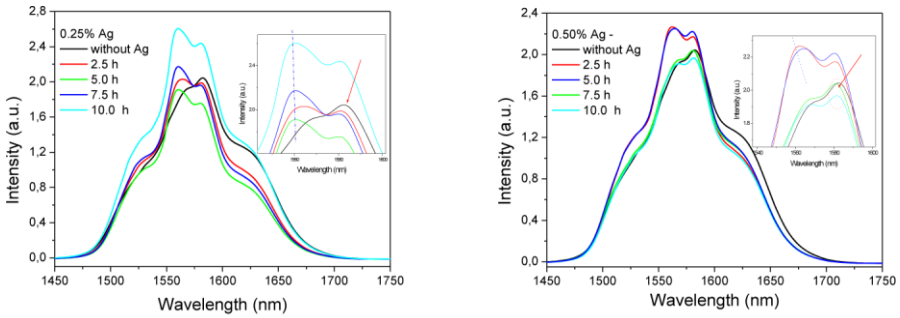

(a) (b)

Fig. 2. (a) Photoluminescence of the TE025-Y samples pumped with diode laser at 980 nm, showing photoluminescence enhancement. The inserted figure shows a zoom of the peaks. The vertical dashed line is a reference for showing the blue-shift of the peaks, and the arrow indicates the enhancement due to transfer energy from EDs to Er^{3+}. (b) Same for the samples TE050-Y. The enhancement of luminescence was found to be reproducible for all ours samples.

where V_{crys} is the crystalline field responsible for the Stark levels and treated as a perturbation, ϕ_i and ϕ_f have the same parity, ϕ_β has opposite parity in relation of ϕ_i and ϕ_f, $\vec{P}$ is the ED from the light interaction. In this sense, Er^{3+} ions presented an electronic configuration $[Xe]4f^{11}$, with J = 15/2 been the spin-orbit ground state because the f shell is more than half-filled. In a weak tetrahedral crystal field, the spin–orbit manifolds split into a number of Stark levels (Γ6, Γ7 and Γ8). The order of these Stark levels depends on the strength of the crystal field and the influence of $\vec{P}_{NP}$, as shown schematically in Fig. 3. This can be verified by the photoluminescence spectra of the samples TE025-10 and TE050-(2.5 and 5.0) [Fig. 2(a) and 2(b) respectively], showing an enhancement of the corresponding peaks. For Er^{3+} ions, the J manifold splits into (2J + 1)/2 Stark levels taking into account the Kramer's degeneracy. The central positions of the Stark levels were obtained by spectrum deconvolution with a fitted Gaussian curve, and listed in Table 2.

In this scenario, the influence of $\vec{P}_{NP}$ appeared in the fluorescence spectrum as a blue-shift of the peaks, e.g. a transfer energy from the NPs dipoles to Er^{3+} ions, thus modifying the Stark energy level's bandwidth, see Fig. 3 (obtained through spectral deconvolution with a fitted Gaussian curve). This energy transfer is obtained from the second term added in Eq. (1) and can be understood through the following definition: $D^{(1)}_{q' Ag-NP} = \sum_m r_m C^{(1)}_{q' Ag-NP}(\theta_m, \varphi_m)$, where $C^{(1)}_{q' Ag-NP}(\theta_m, \varphi_m)$ is the Racah tensor and where r_m is the distance between the NPs and the Er^{3+} ions ($r_m = |\vec{x}|$). This means that the role of the co-dopants is not related to the variation of the character of the wave functions (even or odd) but with transition intensities and probabilities within the f shell.

#134395 - $15.00 USD Received 31 Aug 2010; revised 11 Oct 2010; accepted 14 Oct 2010; published 19 Nov 2010

Table 2. Positions of the Er^{3+} Stark levels taken from absorption and luminescence spectra at ambient temperature (cm^{-1}). The shown values are the average for each concentration of Ag with the different annealing times

Manifold levels	Sample: TE025-Y	Sample: TE050-Y
$^4I_{15/2}$	0 ± 0.81	0 ± 0.46
	67.31 ± 2.36	69.17 ± 2.71
	267.38 ± 1.20	273.21 ± 3.07
	438.92 ± 0.76	442.25 ± 3.12
$^4I_{13/2}$	6563.50 ± 0.22	6567.9 ± 2.62
	6414.15 ± 0.77	6416.58 ± 3.12
	6312.01 ± 1.55	6313.36 ± 1.96
	6150.05 ± 1.65	6150.71 ± 1.66

The Fig. 2(a) and 2(b), shows the enhancement luminescence from effective electric field which is directly connected to the quality factor of the LSP and SPR, e. g. LSPR. This is determined both by intrinsic properties of the NPs via the wavelength-dependent dielectric function of the glass and by the surface effect on the electronic response [14]. As the LSPR properties are sensitive to its environment in the order of its size [15], the dielectric function of the glass containing the NPs express the LSPR bandwidth and resonance frequency. It can be written as the sum of the bound and quasi-free (conduction) electron contributions [16]: $\varepsilon(\omega)=\varepsilon^{ib}(\omega)-\omega_p{}^2/\omega[\omega+i\gamma]$, the bound electron contribution ε^{ib} remains unchanged [17]. A similar expression can be used for the contribution of conduction electrons [18]: $\gamma=1/\tau^{NP}=1/\tau_0+2g_sV_F/d$. Where the first term, $1/\tau_0$ is associated to bulklike electron scattering process in the particle and the second term is a consequence of quasi-electron-free interaction with the surface and, for a sphere, V_F is the Fermi velocity, and g_s is the surface factor [16].

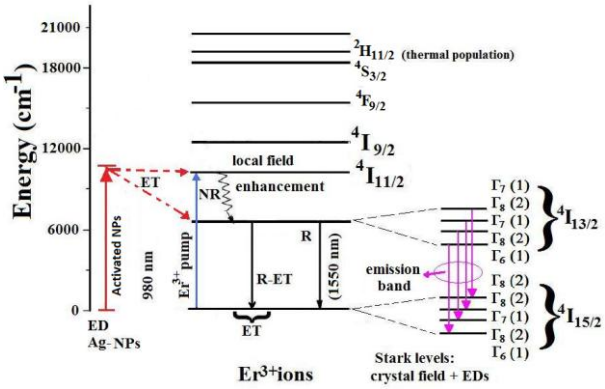

Fig. 3. Energy diagram of the Er^{3+} showing the splitting of levels due to electron-electron (Coulomb) interaction take place the ^4I terms, spin-orbit interaction yielding the manifolds J = 15/2, 13/2, 11/2 and 9/2 and the Stark levels induced by crystal field of tetrahedral symmetry. Also is indicated the process of radiative and non-radiative energy transfer from the pump to ED, and from the pump to Er^{3+}. ET: energy transfer, R: radiative, NR: non-radiative.

We can see the dependence of the LSPR damping factor g that produce a quenching on the luminescence [TE025-(2.5 and 5.0) and TE050-(7.5 and 10.0)] as the effective electric field is a function of g and q which in turn depend on d. This dependence only permits enhancement fluorescence for the samples TE025-10.0 and TE050-(2.5 and 5.0), whose size range is 17.0 < d < 20.0 nm. Furthermore, is verified from the absorption spectrum [pictures into Fig. 1 (a)] that $l_{P\text{-}TE025\text{-}Y}$ = 790 ± 3 nm and $l_{P\text{-}TE050\text{-}Y}$ = 548 ± 3, this values are obtained through the plasma frequency: $\omega_p=\sqrt{4\pi ne^2/(\varepsilon_0\varepsilon_d(\omega)m^*)}$, where n is the charge carrier density, e is the

#134395 - $15.00 USD Received 31 Aug 2010; revised 11 Oct 2010; accepted 14 Oct 2010; published 19 Nov 2010

electron charge, $\varepsilon_d(\omega)$ is the dielectric permittivity in function the excitation frequency ω, and *m** is the electron mass.

The silver's dielectric constant has a very small imaginary part and very high electrical conductivity, which leads to excellent optical and electronic properties of Ag nanostructures, which have motivated us to study silver NPs embedded in a dielectric matrix, with the aim to achieve strong light absorption in a broad spectral region. The luminescence spectrum of Fig. 2(a) and 2(b) shows a blue-shift due to the size dependence of the LSPR (see Fig. 4).

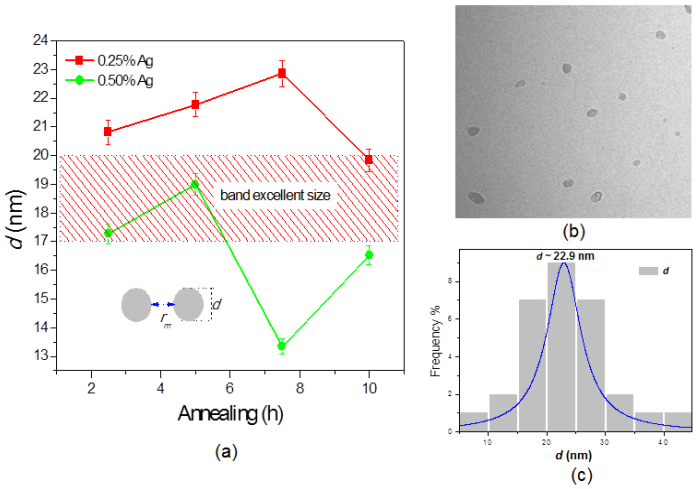

Fig. 4. Calculated NPs' diameter (*d*) of the NPs versus annealing time to samples both TE025-Y and TE050-Y samples. The inserted figures are a schematic representation of one ED, showing it size *d* and separation distance r_m. (b) The 600 × 600 nm^2 TEM photograph of the Ag NPs (TE025-10.0) show closely dispersed particles, the majority of which are ellipse shape. The maximum length (major axis) of the NPs varies from 19 to 23 nm and aspect ratio 1.0–1.2. (c) Histogram of Ag NPs size from picture (b).

The enhancement luminescence intensity is related to the strong local electric field induced by NPs ED, increases the quantum yield h of the luminescence, defined by the ratio of the local field $\vec{E}_{loc}$ and the incident field $\vec{E}_i$, $\eta = (r_m + d)/d = |\vec{E}_{loc}|/|\vec{E}_i|$ [4], here $\vec{E}_{eff} = \vec{E}_{loc} + \vec{E}_i$. Thus the maximum field enhancement is determined by the shortest distance between two equipotential particles. Table 1 clearly shows that as the relative separation (d/r_m) between the Ag NPs increases, h decreases. It corroborates well with the demonstration of Tirtha Som [4] and Le et al. [19]. In the present study, the maximum luminescence enhancement has been observed in the range, $0.11 < r_m/d < 0.12$, for the sample TE050-Y and $r_m/d \approx 0.10$ for the sample TE025-10.0. The field enhancement factor range was $9.18 < \eta < 10.03$ for TE050-Y and $\eta = 10.60$ for TE025-10.0. The size of the particles calculated from the Scherre's formula, are show in the Fig. 4(a).

The growth process of the NPs involves several steps which includes the formation, diffusion, and adsorption of growth species Ag^+ onto the growth surface, and subsequent incorporation of this adsorbed species into the bulk. A diffusion-limited growth causes a different size distribution of NPs, Fig. 4(b) and 4(c). In this sense, the ions Ag^+ are produced during the melting process and the NPs growth occurs when the glass is annealed at 300 °C (above T_g), when the glass viscosity is sufficient to promote the Ag^+ diffusion. If the NPs start to growth at different times, or the Ag^+ ions are non-homogeneously distributed into the glass, we can expect a broad distribution of NPs size, see Fig. 4(c).

It's important to note that, the samples TE025-Y and TE050-Y show prominent diffraction peaks of Ag at $2\theta = 44.8 \pm 0.4°$ ($d' = 2.0231 \pm 0.0169$ Å), which corresponds to the (hkl -

#134395 - $15.00 USD Received 31 Aug 2010; revised 11 Oct 2010; accepted 14 Oct 2010; published 19 Nov 2010

200) diffraction planes of Ag crystals [20]. By XRD analysis we can verify the complete reduction of Ag^{+} to Ag^{0} with annealing, without any formation of silver oxides, such as Ag_2O (Ag^{+}), Ag_2O_3 (Ag^{3+}), or AgO (Ag^{2+}).

Other effect produced by the presence of NPs is the decreasing in the $^4I_{13/2}$ lifetime (see Fig. 5(a)] due to nonradiative energy transfer after the incidence of the pump energy [l = 980 nm) to excite the NPs, yielding LSPR that can be adjusted by the size of the NP (see Fig. 5). This effect contrast with the absorption spectra of the samples (see Fig. 1), who shows that the more the absorption, the less the lifetime is. Mathematically, the radiative lifetime τ_r can be derived from the Judd-Ofelt equation [13,21]: $1/\tau_r = \sum_J A_{J',J}$, where $A_{J',J}$ is the transition probability for any excited state transition ($J' \rightarrow J$). This means that an increment in the absorption is due to the presence of NPs and results a lifetime decrease. In particular the samples TE025-5.0 and TE050-10.0 shows an absorption enhancement with the increment of NP size [Fig. 5(b)]. In addition, the lifetime also arise from the increase of radiative decay rate Γ_R ($=1/\tau_r = \Gamma_{all} = \Gamma_R + \Gamma_{NR}$) due the presence the NPs with a little g that is favorable, such as in samples TE025-10, TE050-2.5, TE050-5.0 where photoluminescence intensity is improved from the Ag NPs presence [Fig. 2(a) and 2(b)].

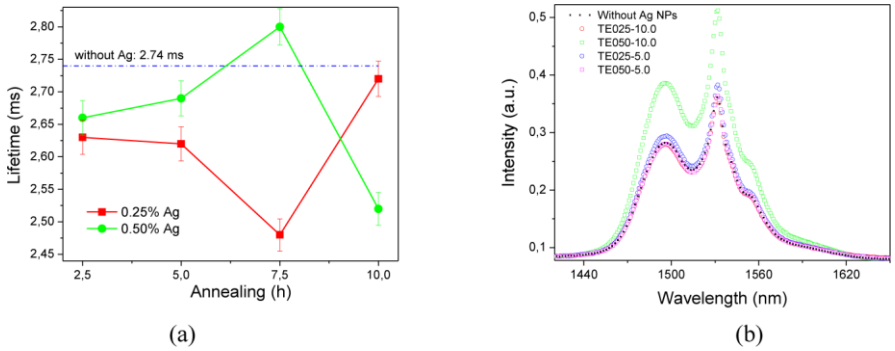

Fig. 5. Lifetime of the $^4I_{13/2}$ level for all samples, as compared with the lifetime of the sample without NP (dashed line). The bars indicate errors of ± 2%. (b) Absorption spectra show the increasing absorption due to the presence of silver NPs.

4. Conclusion

In summary, we have shown that Er^{3+}-doped tellurite glass are a good host matrix that permitted the formation and the diffusion of NP into the host in function of the annealing time in comparison others [4,7,19 and 22,], inducing the formation of EDs that are activated by the energy transfer between the Er^{3+} ions and the NPs, forming LSPR, by non radiative energy transfer and consequently causing a decrease in the $^4I_{13/2}$ lifetime of ours samples. The effective field turns out to be $\vec{E}_{eff} = \vec{E}_{loc} + \vec{E}_i$. The EDs cause a great enhancement of the Er^{3+} $^4I_{13/2} \rightarrow {}^4I_{15/2}$ transition due to the energy transfer from the ED to the Er^{3+}, which depends on the ratio d/r_m as evidenced by a blue-shift of the luminescence peaks. Besides, the presence of NPs into the host did not modify the crystalline field, but it is responsible for the changes in the energy of Stark levels as indicated in Eq. (1). This significant enhancement in the fluorescence has a potential application in amplifiers waveguide for plasmonic devices. The most exciting feature of this work is that the fabrication process is very simple and it can be potentially scaled up to mass production of amplifiers and other photonic devices.

Acknowledgements

This work was financially supported by the Brazilian agencies Fapesp, CNPq, INOF. We are grateful to Agusto L. da Rocha for technical support provided X-ray measurements.

#134395 - $15.00 USD Received 31 Aug 2010; revised 11 Oct 2010; accepted 14 Oct 2010; published 19 Nov 2010